ROYAL SOCIETY
OF CHEMISTRY

Check for updates

A sweat-pH-enabled strongly adhesive hydrogel for self-powered e-skin applications†

Lei Zhang, [ab] Siheng Wang, [a] Zhuomin Wang,[a] Zhen Huang,[b] Penghao Sun,[b] Fuhao Dong,[a] He Liu, *[a] Dan Wang*[a] and Xu Xu *[b]

On-skin hydrogel electrodes are poorly conformable in sweaty scenarios due to low electrode–skin adhesion resulting from the sweat film formed on the skin surface, which seriously hinders practical applications. In this study, we fabricated a tough adhesive cellulose-nanofibril/poly(acrylic acid) (CNF/PAA) hydrogel with tight hydrogen-bond (H-bond) networks based on a common monomer and a biomass resource. Furthermore, inherent H-bonded network structures can be disrupted through judicious engineering using excess hydronium ions produced through sweating, which facilitate the transition to protonation and modulate the release of active groups (*i.e.*, hydroxyl and carboxyl groups) accompanied by a pH drop. The lower pH enhances adhesive performance, especially on skin, with a 9.7-fold higher interfacial toughness (453.47 *vs.* 46.74 J m^{-2}), an 8.6-fold higher shear strength (600.14 *vs.* 69.71 kPa), and a 10.4-fold higher tensile strength (556.44 *vs.* 53.67 kPa) observed at pH 4.5 compared to the corresponding values at pH 7.5. Our prepared hydrogel electrode remains conformable on sweaty skin when assembled as a self-powered electronic skin (e-skin) and enables electrophysiological signals to be reliably collected with high signal-to-noise ratios when exercising. The strategy presented here promotes the design of high-performance adhesive hydrogels that may serve to record continuous electrophysiological signals under real-life conditions (beyond sweating) for various intelligent monitoring systems.

New concepts

Self-powered skin-attachable electronics are under intense development to enable the internet of everything and everyone in new and useful ways. Self-powered electronic skins (e-skins) based on adherent hydrogels that serve as electrodes are attracting increasing levels of attention because they are non-invasive and easily applied, while also eliminating the restraints of external power supplies and the need for medical tape, which are distinct advantages. While hydrogel-based self-powered e-skins are used in healthcare, sports-management, and modern lifestyle applications, current on-skin hydrogel electrodes perform poorly on sweaty skin due to low electrode–skin adhesion, which seriously hinders practical applications. Based on the above concept, we overcome this problem by turning the perceived intrinsic flaws of sweat into merits by fabricating a tough adhesive cellulose-nanofibril/poly(acrylic acid) (CNF/PAA) hydrogel with a tight hydrogen-bond (H-bond) network. The developed hydrogel exhibited enhanced adhesion at lower pH (akin to sweat), especially on skin. This is promising for self-powered e-skins.

Introduction

Electronic skins (e-skins) are wearable epidermal devices that combine the stretchability and softness of human skin with

additional features, and have been widely used in bioinformatics monitoring and healthcare ecosystem applications.[1–5] Self-powered e-skins based on adhesive hydrogels that serve as electrodes are attracting increasing levels of attention because they are non-invasive and easily applied, while also eliminating the restraints of external power supplies and the need for medical tape,[6–10] which are distinct advantages. However, sweating, which is inevitable under real-life conditions, especially during prolonged monitoring and exercise, is seldom considered; such conditions require hydrogel-based on-skin electrodes that remain conformable and adhesive in the presence of sweat.[11] Unfortunately, current non-invasive electrodes are poorly conformable

[a] *Institute of Chemical Industry of Forestry Products, Key Laboratory of Biomass Energy and Material, Jiangsu Province, Key Laboratory of Chemical Engineering of Forest Products, National Forestry and Grassland Administration, National Engineering Research Center of Low-Carbon Processing and Utilization of Forest Biomass, Jiangsu Co-Innovation Center of Efficient Processing and Utilization of Forest Resources, Chinese Academy of Forestry, Nanjing 210042, China. E-mail: liuhe.caf@gmail.com, wgdan@163.com*

[b] *College of Chemical Engineering, Jiangsu Co-Innovation Center of Efficient Processing and Utilization of Forest Resources, Nanjing Forestry University, Nanjing 210037, China. E-mail: xuxu200121@njfu.edu.cn*

and adhere less to sweaty skin due to the formation of a sweat film with low shear viscosity on the skin surface, which disrupts molecular interactions between the skin and the adhesive,[12–16] leading to detachment of the electrode from the skin. For example, commercial gel electrodes tend to slip off sweaty skin, resulting in false and even missing signals.[17–20] To address this issue, hydrogel electrodes must maintain their conformal and adhesive properties in the presence of sweat to ensure stable long-term dynamic physiological monitoring.

Several design approaches have been proposed for the development of tough adhesive hydrogels for use on sweaty skin, including introducing catechol groups (inspired by mussels), constructing semi-interpenetrating or double-network structures, and creating metal coordination or chelation interactions, among others.[21–23] Unfortunately, these methods inevitably involve energy-intensive operations and complicated procedures, as well as harsh processing conditions. For example, preparing common mussel-inspired hydrogels with tough adhesive properties often requires complex activities or conditions.[24] More notably, design strategies for such tough adhesive hydrogels usually avoid the spontaneous inherent defects of sweaty skin, which inevitably excludes the virtues of sweat, including the dynamic pH and salt concentrations (Na$^+$, K$^+$, *etc.*) provided by sweat during exercise.[25,26] Turning the perceived intrinsic flaws of sweat into merits is a challenging strategy worth considering. A healthy person produces sweat with a pH that is well-known to lie in the 4.5–7.5 range; sweat pH tends to decrease when engaged in sports or when exercising,[27–30] which provides a dynamic parameter for the development of a tough adhesive hydrogel. Conversely, we envisage that a sweat-pH-enabled hydrogel that adheres more when sweating or exercising can be developed and applied to self-powered e-skins for long-term personal-health monitoring.

In this study, we developed a design strategy for polymer hydrogel electrodes that involves the *in situ* polymerization of acrylic acid (AA), a common monomer, and cellulose nanofibrils (CNFs) to produce an approximately pH-neutral cellulose nanofibril/poly(acrylic acid) (CNF/PAA) hydrogel. CNFs are abundantly available from a variety of biomass resources (*i.e.*, wood) and are rich in oxygen-containing polar functional groups (*i.e.*, hydroxyl and carboxyl groups) in the form of repeating glucose units.[31] These polar functionalities facilitate the formation of tight hydrogen bonds (H-bonds) with the carboxyl groups derived from poly(acrylic acid) (PAA), thereby enabling the hydrogel to strongly and toughly adhere to skin. Furthermore, sweat pH is used to promote protonation and disrupt the H-bonded network structure of the hydrogel in a controlled manner through structural-design engineering, leading to the release of more free and active hydrophilic groups that boost robust adhesion. Tight adhesion is maintained and the hydrogel electrode does not detach from sweaty skin, even at persistently low sweat pH; this process amplifies the advantages of sweat for enhancing adhesion (Fig. 1a). Non-destructive detachment of the hydrogel electrode from the skin at high pH is still realized based on strong coupling between the hydrogel electrode and the skin interface at low pH

(Fig. 1b). The interfacial toughness of our obtained hydrogel exceeds 450 J m^{-2} on sweaty skin, which is 4.5-times that of commercial VHB tape owing to tough adhesion; hence, the hydrogel is a strong potential candidate for use in e-skin applications (Fig. 1c). Notably, the fabricated hydrogel exhibits excellent mechanical properties over the entire pH range of sweat, and the hydrogel maintains outstanding adhesion and toughness at relatively low sweat pH (pH < 5), while the hydrogel at moderate sweat pH (pH 5–7) is stretchable and resilient, as well as exhibits rigidity and robustness at relatively high pH (pH > 7), highlighting impressive pH controllability that meets the application requirements of various scenarios (Fig. 1d). Combined with desirable tunability, the strategy presented herein facilitates the design of high-performance adhesive hydrogel electrodes for use in self-powered e-skins and other applications.

Results and discussion

pH control over CNF/PAA hydrogel micromorphology and H-bonding

We used *in situ* confocal laser scanning microscopy (CLSM) to capture subtle changes in the microstructures of fluorescent-dye-stained CNF/PAA hydrogels prepared at various pH values. Large-area aggregated fluorescent regions were observed to transform into relatively dispersed states with decreasing pH, indicative of hydrogel polymer backbone loosening due to disruption of the inherent H-bond network (Fig. 2a), consistent with scanning electron microscopy (SEM) observations. Compared with the smooth surface observed for the initial dry CNF/PAA hydrogel, numerous dense micropores appeared with decreasing pH, which suggests that a porous architecture is formed (Fig. 2b). These favourable results can be further demonstrated by the appreciable swelling properties of hydrogels including deionized water and artificial sweat with varying pH values (Fig. S1 and S2, ESI†). Taken together, the fluorescence and imaging techniques show that free hydronium ions tend to disrupt the original H-bond network in the hydrogel, which contributes to polymer-chain self-dissociation.

We next analysed the microstructural features of the CNF/PAA hydrogel at the molecular level using *in situ* small-angle X-ray scattering (SAXS) and low-field (LF) nuclear magnetic resonance (NMR) techniques (Fig. 2c–e), which revealed that the scattering peak at $q \approx 0.008$ Å^{-1} in the spectrum of the hydrogel weakens with decreasing pH, consistent with the formation of a dispersible microstructure (Fig. 2c and Fig. S3, ESI†).[32] Moreover, the free water relaxation time (T_2) was observed to shift to higher field, which indicates that the water molecules in the hydrogel system become more mobile, in good agreement with the higher free water content at relatively low pH (Fig. 2d and Fig. S4, ESI†).[33] Taken together, these impressive results reveal the presence of a sensitive microstructural transition; *i.e.*, a dense microstructure exists at relatively high pH (*i.e.*, 7.5), whereas a loose microstructure generated by the hydronium-ion-induced collapse of the H-bonded network exists at relatively low pH (*i.e.*, 4.5).
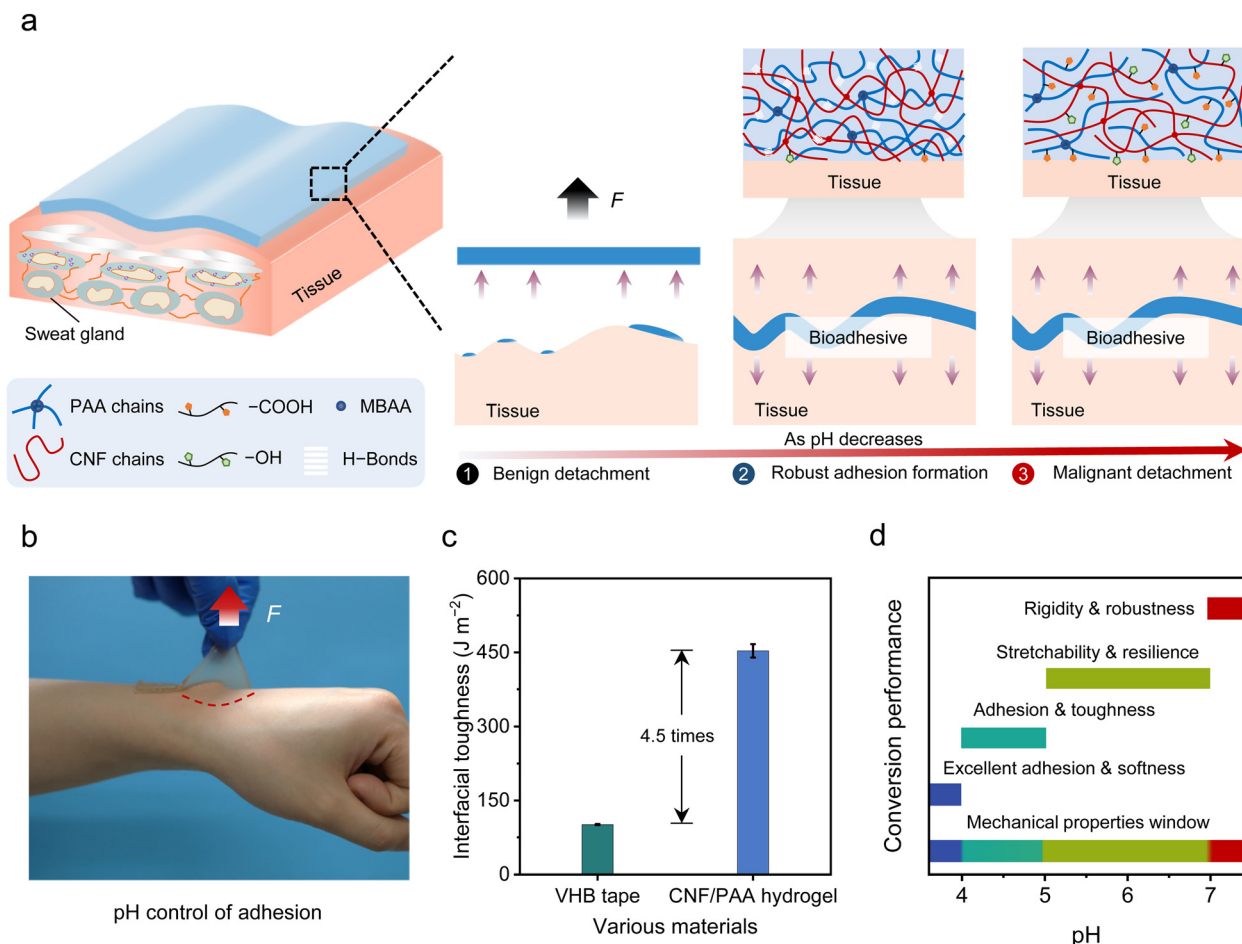
Fig. 1 Design of a sweat-pH-triggered strong adhesive hydrogel. (a) Schematic illustrating the CNF/PAA hydrogel design. (b) Photographic image of the CNF/PAA hydrogel peeled from human skin. (c) Comparing the interfacial toughness of the CNF/PAA hydrogel and commercial VHB tape on sweaty skin with pH 4.5. (d) Mechanical and adhesive gradations of CNF/PAA hydrogels at various pH values.

To gain further insight into the effect of hydronium ions on the CNF/PAA hydrogel, we used two-dimensional (2D) Raman spectroscopy, Fourier-transform infrared (FTIR) spectroscopy, and X-ray photoelectron spectroscopy (XPS) to investigate the H-bond interactions in the hydrogel at various pH values (Fig. 2f–i). The 2D Raman map shows the peak associated with the carbonyl group (C=O) at 1698 cm^{-1}, where the change in the intensity of the peak with decreasing pH conditions is represented from the left to the right of the mapping; the blue-green regions in the map correspond to areas of relatively low intensity, while yellow-red corresponds to relatively high intensity, and the scale on the right is the peak intensity range. (Fig. 2f and Fig. S5, ESI†).[34] This interesting observation indicates that the abundant hydronium ions in the hydrogel system disrupt the inherent H-bonded network, resulting in the release of more free C=O; it also reveals that the H-bond interactions in the hydrogel weaken. More intuitively, the peak attributable to C=O at 1735 cm^{-1} in the FTIR spectrum can be deconvoluted into two representative peaks, namely one corresponding to free C=O (peak I) and the other to H-bonded C=O (peak II), as shown in Fig. 2g. We found that the intensity of peak I decayed significantly with decreasing pH, which is a

good indicator that an abundance of free C=O moieties is produced. Concomitantly, peak II exhibits an obvious blue shift, consistent with subdued H-bond interactions in the hydrogel network.[35] Furthermore, XPS revealed that the O–C–O/COOH (C 1s), O=C–O, and C–O–C/C–O–H (O 1s) peaks shift to higher binding energies with decreasing pH, which suggests that hydronium ions weaken H-bond interactions (Fig. 2h and i).[34] Additionally, the infrared spectra of the dried hydrogel show enhancement of the C=O stretching band of –COOH at 1648 cm^{-1} and diminishing asymmetric and symmetric –COO$^-$ stretches at the respective 1545 and 1402 cm^{-1} as pH decreases, suggesting the formation of protonated states.[36–38] Overall, the above results lead us to conclude that excess hydronium ions weaken the H-bonded network in the hydrogel system at relatively low pH (*i.e.*, 4.5), resulting in a conversion in protonation and the release of more free oxygen-containing functional groups (such as –COOH and –OH), thereby enabling the formation of polymer-chain architectures with large numbers of hydrophilic active sites on their surfaces.

Mechanical performance of the CNF/PAA hydrogel

The CNF/PAA hydrogel deformed little when subjected to an external force at a relatively high pH (*i.e.*, 7.5) owing to its
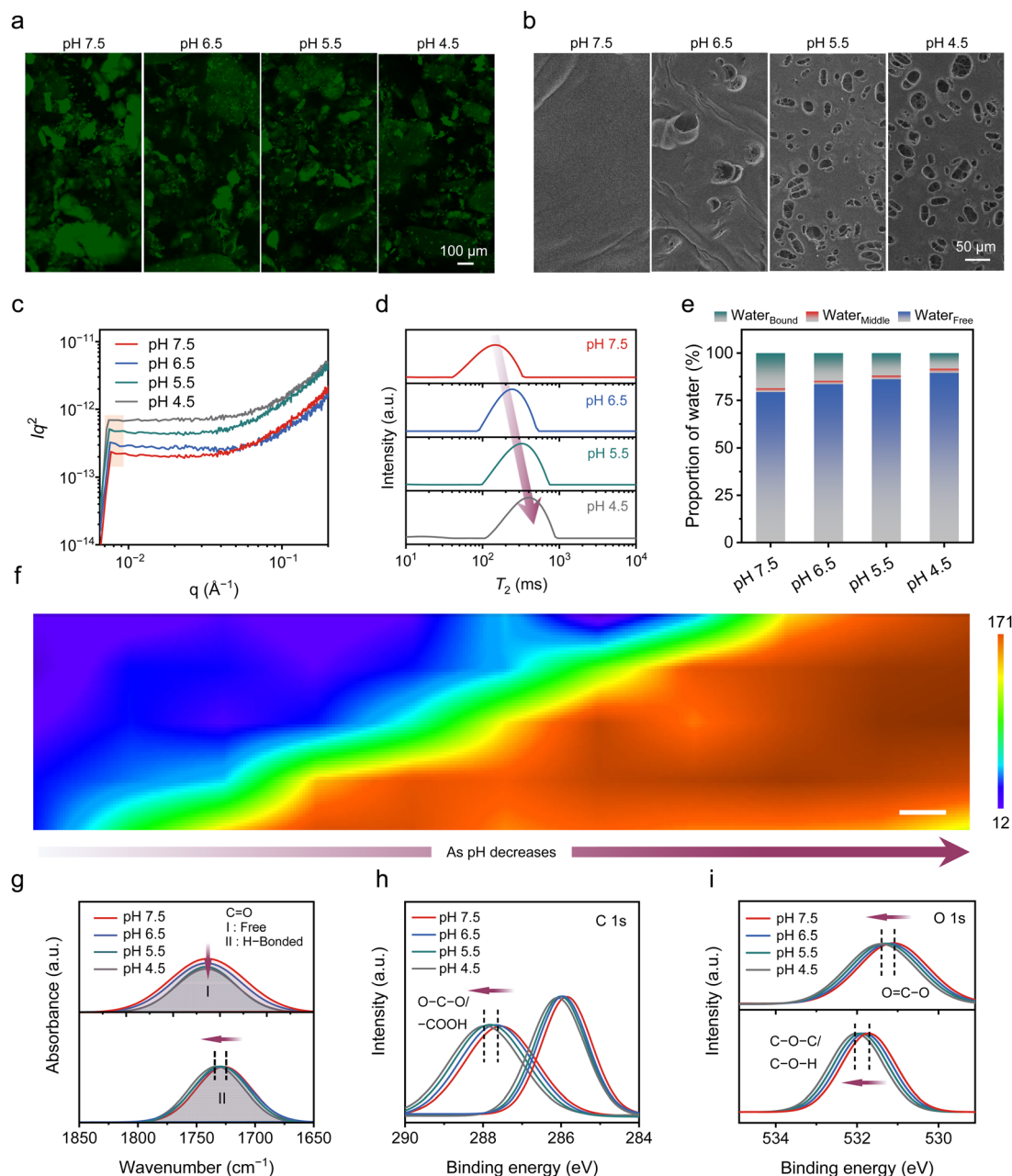
Fig. 2 Sweat-pH-induced tuning of the CNF/PAA hydrogel micromorphology and its H-bond structure. Continuous (a) CLSM and (b) SEM images of equilibrating CNF/PAA hydrogels at pH 7.5–4.5. (c) SAXS spectra of the CNF/PAA hydrogel at pH 7.5–4.5. (d) LF-^{1}H NMR spectra of the CNF/PAA hydrogel at pH 7.5–4.5. (e) Proportions of water in the CNF/PAA hydrogel at various pH values (7.5–4.5). (f) 2D Raman mapping associated with the intensity of the peak at 1698 cm^{-1} belonging to the carbonyl group (C=O) with decreasing pH conditions. The blue-green regions in the mapping correspond to areas of relatively low intensity, while yellow-red corresponds to relatively high intensity. Scale bar, 10 μm. (g) Deconvoluted FTIR peaks at 1730 and 1740 cm^{-1} corresponding to the CNF/PAA hydrogel at pH 7.5–4.5. (h) C 1s and (i) O 1s XPS spectra of the CNF/PAA hydrogel at pH 7.5–4.5.

compact H-bond network, indicative of high stiffness. In sharp contrast, the hydrogel is easily stretched, bent, and compressed without significant chipping or fracturing in its relatively low pH state (*i.e.*, pH 4.5) owing to disruption of the H-bond network by the excess hydronium ions present in the hydrogel, suggestive of excellent conformability and ductility (Fig. 3a–c).

Tensile and compression testing were used to further investigate the effect of pH on the mechanical properties of the

CNF/PAA hydrogel by quantitatively analysing its mechanical performance. Fig. 3d reveals that the tensile strength and fracture strain of the CNF/PAA hydrogel exhibit opposite trends with decreasing pH. The hydrogel exhibited an ultimate stress of 0.084 MPa and a fracture strain of 315% at pH 7.5; however, the ultimate stress decreased by 73.8% (to 0.022 MPa) and the fracture strain increased by a factor of 5.7 (to 1800%) when the pH was reduced to 4.5; these observations are attributable to
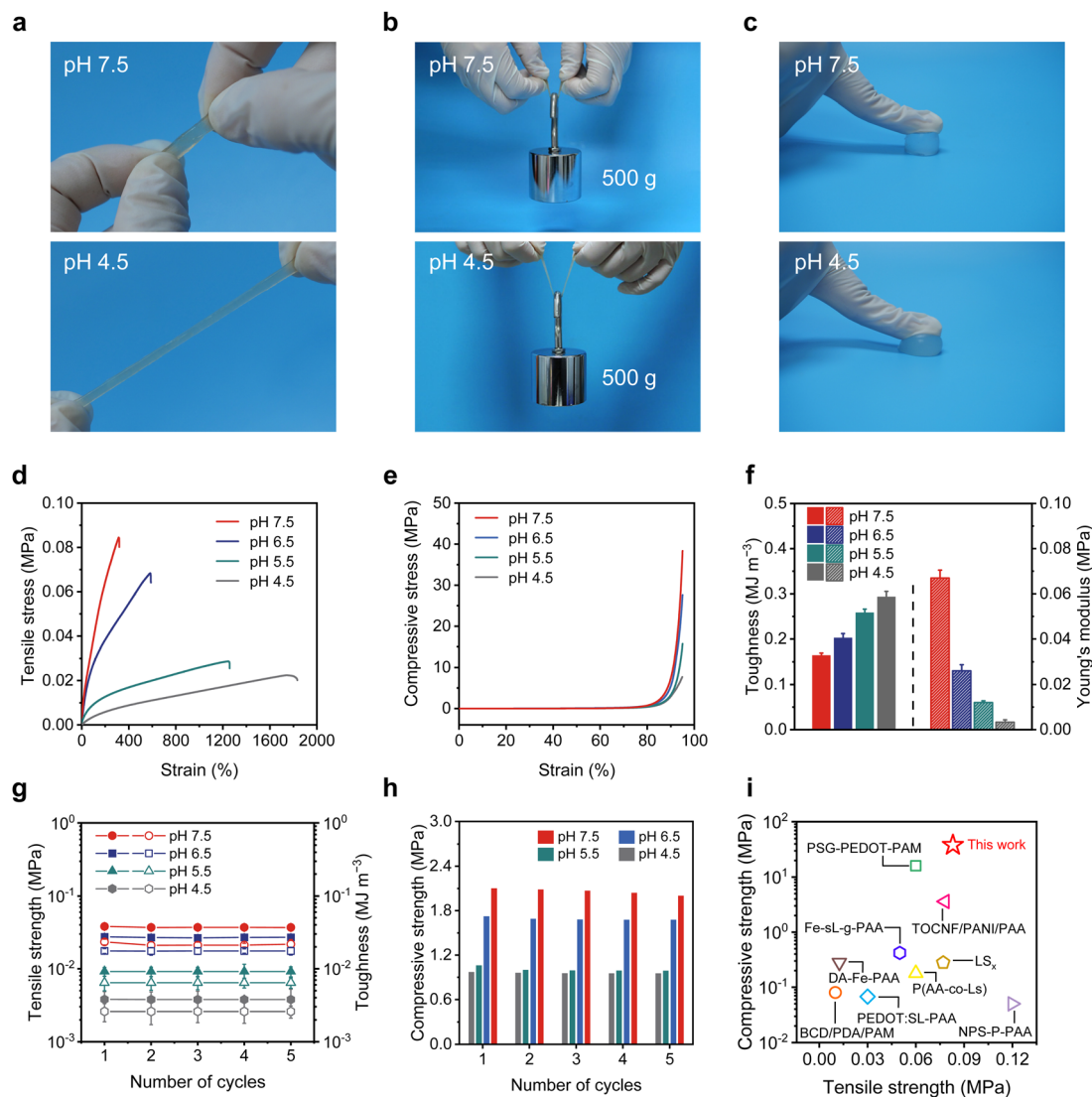
Fig. 3 Mechanical properties of the CNF/PAA hydrogel at pH 7.5–4.5. (a) Comparison of photographs of the CNF/PAA hydrogel stretched under external force at pH 7.5 and 4.5, respectively. (b) Comparison of photographs of the CNF/PAA hydrogel suspended by a 500 g weight at pH 7.5 and 4.5, respectively. (c) Comparison of photographs of the CNF/PAA hydrogel squeezed by a finger at pH 7.5 and 4.5, respectively. (d) Tensile and (e) compressive stress–strain curves for the CNF/PAA hydrogel at pH 7.5–4.5. (f) Toughness and Young's modulus values for the CNF/PAA hydrogel at pH 7.5–4.5. Data are presented as the means ± SDs (n = 3). (g) Cyclic tensile strength and toughness values for the CNF/PAA hydrogel at pH 7.5–4.5. Data are presented as the means ± SDs (n = 3). (h) Cyclic compressive strengths of the CNF/PAA hydrogel at pH 7.5–4.5. (i) Mechanical properties of the CNF/PAA hydrogel with pH 7.5 and other reported materials.

the weakening of the H-bond network induced by excess hydronium ions (Fig. S7, ESI†). Compressive stress–strain testing revealed that compressive strength exhibits a similar decreasing trend with decreasing pH; for example, a compressive strength of 38.39 MPa was observed at pH 7.5, while it was only 7.69 MPa at pH 4.5, which corresponds to a 79.9% decrease (Fig. 3e). As expected, a similar mechanical behavior was exhibited for the compressive stress at a strain of 80%; that is, the corresponding stress decreases from 0.81 MPa to 0.66 MPa, accompanied by a drop in pH from 7.5 to 4.5 (Fig. S9, ESI†). Notably, the fracture toughness and tensile modulus of the hydrogel show opposite trends with decreasing pH, with a high fracture toughness of 0.29 MJ m^{-3} and a good tensile

modulus of 0.0033 MPa observed at a representative pH of 4.5, indicative of excellent robustness and in good agreement with rheological data (Fig. 3f and Fig. S8, ESI†). In addition, it can be found that a controllable wide-range tuning of the hydrogel in mechanical properties can be achieved by adjusting the amount of CNFs (Fig. S10, ESI†).

We next explored the mechanical cycling properties of the CNF/PAA hydrogel. Fig. 3g and Fig. S11 (ESI†) show that the hydrogel exhibits stable tensile strength and toughness, with negligible attenuation observed as the pH was varied during five stretching cycles, indicative of excellent cyclic stretching performance. The hydrogel also exhibited similar compressive mechanical behavior, which highlights its reliable mechanical

durability and stability (Fig. 3h and Fig. S12, ESI†). The combined excellent stretchability and compressibility of our prepared hydrogel reveals that it outperforms most existing adhesive hydrogels, especially in terms of tensile and compressive strength (Fig. 3i and Table S1, ESI†).[39–47]

Adhesion performance of the CNF/PAA hydrogel

Owing to its rich multipolar groups, the CNF/PAA hydrogel steadily adheres to the skin covering human joints, and

exhibits a seamless adhesion interface and stable stretching bands without any visible motion-induced shedding (Fig. 4a). Moreover, the hydrogel was observed to stably adhere to several steel balls (total weight of up to 36 g) and simultaneously lift a weight of 500 g without significant fracturing, thereby demonstrating a combination of excellent adhesion properties and robust toughness (Fig. 4b and Movie S1, ESI†). Surprisingly, two aluminum plates adhered together using the CNF/PAA hydrogel tightly resisted stretching or slipping when a 5 kg weight was
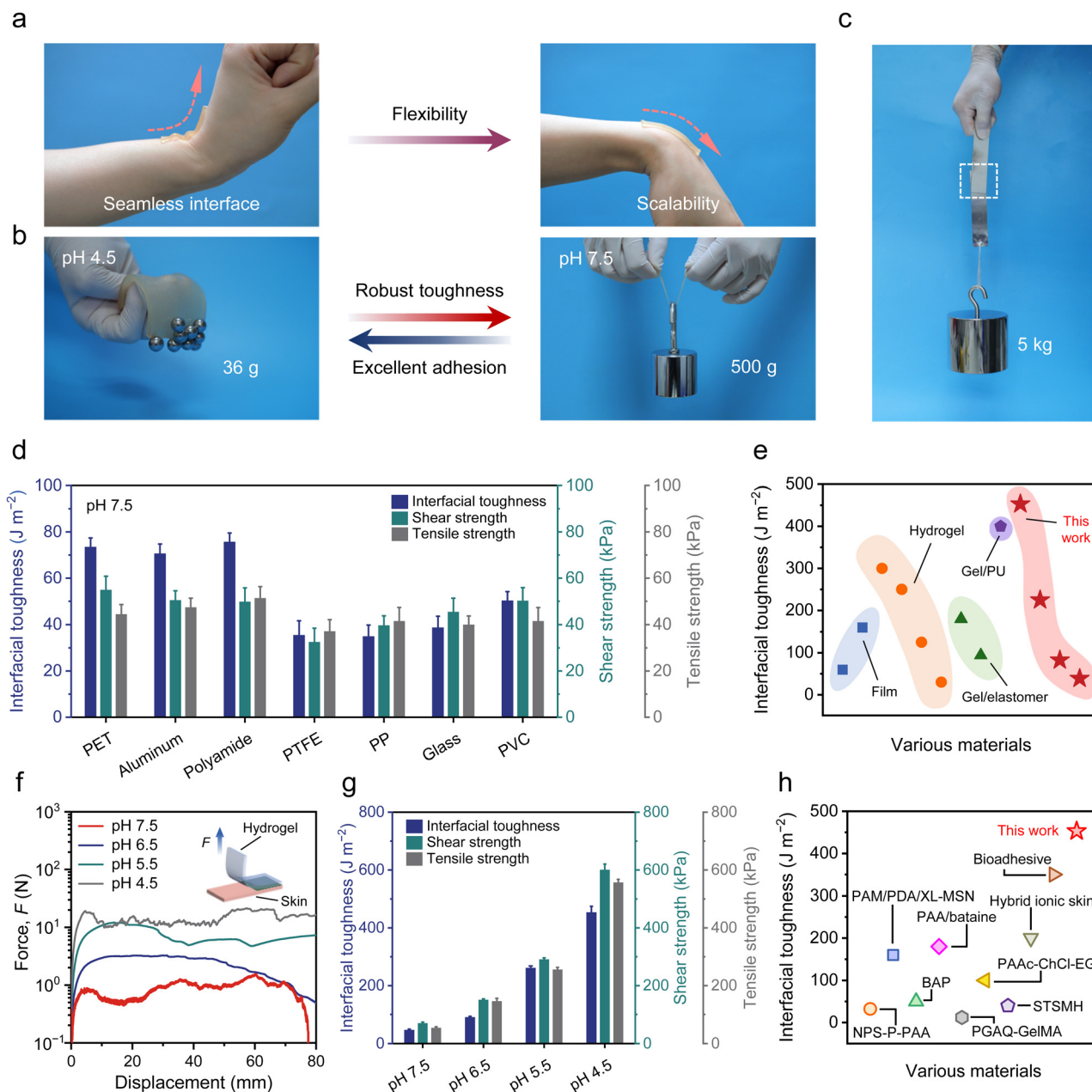

Fig. 4 Adhesive properties of the CNF/PAA hydrogel at pH 7.5–4.5. (a–c) Photographic images showing the excellent adhesive performance of the CNF/PAA hydrogel. (d) Comparing the interfacial toughness, shear strength, and tensile strength of the CNF/PAA hydrogel on various engineering material substrates at pH 7.5. Data are presented as the means ± SDs (n = 3). (e) Adhesive properties of the CNF/PAA hydrogel and other reported materials on glass. (f) Plateau force−displacement curves for the CNF/PAA hydrogel at pH 7.5–4.5. The inset schematically shows the 90 degree peeling test. (g) Comparing the interfacial toughness, shear strength, and tensile strength of the CNF/PAA hydrogel on freshly excised porcine at pH 7.5–4.5. Data are presented as the means ± SDs (n = 3). (h) Adhesive properties of the CNF/PAA hydrogel with pH 4.5 and other reported materials on freshly excised porcine skin.

applied, highlighting the reliable adhering properties of the hydrogel (Fig. 4c). This impressive behavior suggests that the CNF/PAA hydrogel is endowed with the advantages of both toughness and adhesion.

It can be observed that the CNF/PAA hydrogel can be firmly adhered between fingers and other various substrates without visible signs of detachment, which indicates the capability of stably adhesive properties of the hydrogel (Fig. S13, ESI†). Furthermore, we used three adhesion-testing methods to quantitatively investigate the adhesive properties of the CNF/PAA hydrogel, including 90 degree peel testing for interfacial toughness, lap-shear testing for shear strength, and tensile testing for tensile strength (Fig. S14, ESI†). We obtained objective results over the full pH range (7.5–4.5) when the hydrogel was applied to a variety of substrates, which reveals that the hydrogel exhibits general adhesive performance for use in desirable scenarios (Fig. 4d and Fig. S15–S17, ESI†). In particular, an interfacial toughness, shear strength, and tensile strength of 390.01 J m^{-2}, 507.22 kPa, and 355.91 kPa, respectively, were recorded for the hydrogel when applied to conventional glass at pH 4.5 (Fig. S18, ESI†). Compared against existing adhesive engineering materials, including films, hydrogels, and elastomers, our hydrogel is endowed with significant advantages in terms of interfacial toughness when applied to conventional glass (Fig. 4e and Table S2, ESI†).[8,35,48–54]

We further explored the impact of pH on the adhesion properties of the CNF/PAA hydrogel. Fig. 4f shows that the maximum platform peel force increases with decreasing pH when the hydrogel is subjected to 90 degree peel testing on freshly excised porcine skin, with a maximum plateau force of 11.33 N recorded at pH 4.5, which is 9.7-times the value observed at pH 7.5 (1.17 N). Furthermore, the CNF/PAA hydrogel exhibited a 9.7-fold increase in interfacial toughness, an 8.6-fold increase in shear strength, and a 10.4-fold increase in tensile strength on skin as the pH was reduced from 7.5 to 4.5 (Fig. 4g). These interesting results are due to the fact that the decreased pH promotes protonation states and produces a large amount of hydronium ions that destroy the original H-bonded network and lead to the release of more free oxygen-containing groups, thus increasing the adhesion between the hydrogel and the skin. Additionally, the hydrogel exhibited steady interfacial toughness by adjusting its pH with artificial sweat during five peeling-recovery cycles, which highlights its excellent cyclic adhesive properties (Fig. S19, ESI†). In addition to the effect of pH value, we also investigated the effect of temperature on the adhesion properties of hydrogels applied to skin. The interfacial toughness results can be observed revealing that the pH is the most preferential influencing factor for enhancing the adhesion performance of hydrogels compared to the temperature dependence (Fig. S20, ESI†). Surprisingly, even in water, the hydrogel still exhibited an interfacial toughness of 138.64 J m^{-2} at pH 4.5, showing the expected underwater adhesion potential (Fig. S21, ESI†). Notably, due to the positive effect of CNFs on the cohesion of the hydrogel network, a wide range of adhesion properties can be realized by tuning the introduction of varying CNFs (Fig. S22, ESI†).

The observed intriguing adhesion behavior confirms that the CNF/PAA hydrogel toughens as the pH is lowered; hence, increased sweating is expected to provide a positive effect during periods of exercise. To verify our prediction, we detected the change in pH value when a volunteer is running, and found that the pH shows a downward trend with the prolongation of exercise, which is consistent with the results of recent work (Fig. S23, ESI†).[27,28] Also, the interfacial toughness increases to 46.74 J m^{-2} on sweaty skin with pH 7.5 compared to 41.30 J m^{-2} on dry skin, which is in good agreement with our expectations (Fig. S24, ESI†). Finally, the interfacial toughness of our fabricated hydrogel exceeds those of most reported adhesive hydrogel materials on skin; consequently, we expect it to be broadly applicable to e-skin applications and beyond (Fig. 4h and Table S3, ESI†).[8,35,45,53–58]

Applications of the CNF/PAA hydrogel as a self-powered e-skin device

Benefiting from the existence of free ions in the CNF/PAA hydrogel, the hydrogel still maintains excellent conductive performance even under varying pH, with an ionic conductivity of 12.12 mS cm^{-1} at pH 4.5 (Fig. S25, ESI†). In addition, due to the tight H-bonding within the hydrogel, it can achieve self-healing within 30 min at 30 °C without significant decline in ionic conductivity and stretchability (Fig. S26 and S27, ESI†). Surprisingly, even after 6 h at RT (20 °C), the water loss rate of hydrogels is still within 15%, showing trustworthy water retention, which is attributed to the strong interaction between free ions and water in the hydrogel (Fig. S28, ESI†). The CNF/PAA hydrogel was also subjected to biocompatibility testing considering its conformal and intimate contact with human skin during use. The experimental samples showed negligible quantitative differences between live and dead cells; hence, the CNF/PAA hydrogel is highly cytocompatible at various pH values (Fig. S29, ESI†).

Furthermore, when the CNF/PAA hydrogel is adhered to the skin of different volunteers (including female and male), it exhibits stable electrical signal responses during both joint motion and sweating workout, highlighting a potentially ideal conformal, designable, and biocompatible self-powered e-skin candidate for real-world applications during exercise (Fig. S30, S31 and Movies S2, S3, ESI†). As a proof-of-concept demonstration, a single-electrode-mode pH-adhesive detachable triboelectric nanogenerator (pAd-TENG) with a two-layer architecture consisting of a hydrogel and polydimethylsiloxane (PDMS) because of their strong adhesion was designed to demonstrate the potential and reusability of the CNF/PAA hydrogel in an e-skin device (Fig. 5a and Fig. S32–S38, ESI†). The pAd-TENG-based e-skin adheres and conforms to human skin along the highly curved contours of the knuckles, and is easily scaled to produce a large (40 × 50 cm) highly flexible and stretchable device (Fig. 5b and c). A linear relationship was observed between elbow curvature and output voltage of the pAd-TENG-based e-skin when fixed on an elbow to monitor human motion (Fig. 5d). Fig. 5e shows that the e-skin is highly scalable and seamlessly adheres interfacially to human joints
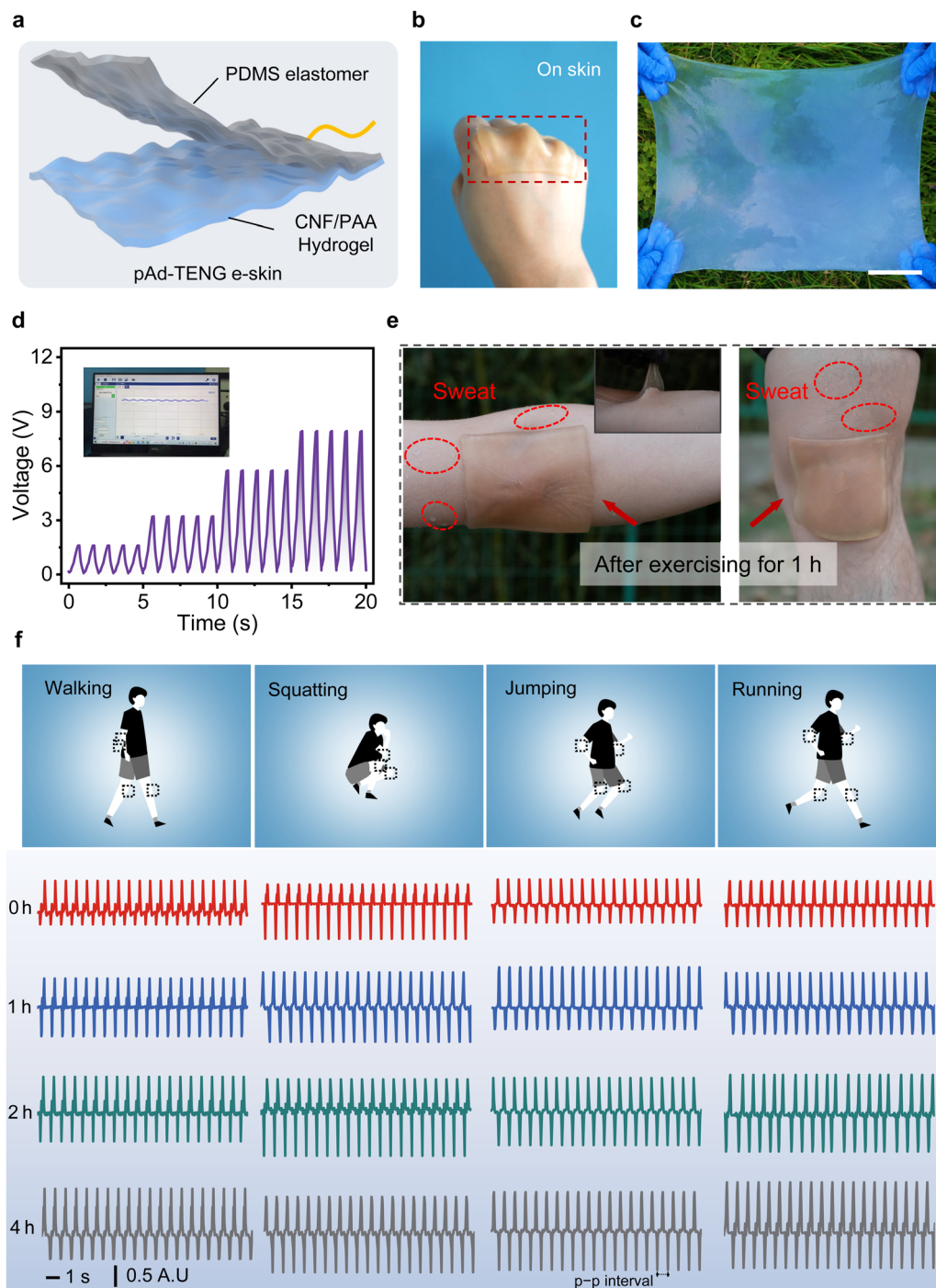
Fig. 5 Skin adhesion and human exercise monitoring using the pH-adhesive detachable triboelectric nanogenerator electronic skin (pAd-TENG-based e-skin). (a) Schematic of the two-layer-structured pAd-TENG. (b) Photographic image of a pAd-TENG-based e-skin attached to a hand. (c) Photographic image of a large area (40 × 50 cm) pAd-TENG-based e-skin. Scale bar: 10 cm. (d) Signal outputs from the pAd-TENG-based e-skin fixed at the elbow at various curvatures during motion. The inset image is the output voltage signal curve obtained by fixing the pAd-TENG-based e-skin on the elbow and maintaining the joint curling degree of 60° for periodic oscillation. (e) Photographic images of the pAd-TENG-based e-skin worn on human arthroses after exercising for 1 h. (f) Detecting human-body exercise from the output voltage signal and corresponding images (the PP interval corresponds to the time between two peaks).

at various large bending strains, even after 1 h of sweating (Fig. S39, ESI†).

Various human body activities were also monitored by mounting pAd-TENGs at various joint positions (Fig. 5f and

Fig. S40, ESI†). A volunteer wore several pAd-TENGs and exercised under various sporting conditions for 4 h. Summary-motion signals of various human body parts were displayed and recorded on a computer screen in real time during exercise, with

maximum amplitude observed during running, which is ascribable to large movements associated with arm swings and leg motions. The amplitudes of recorded human body signals remained stable and slightly increased completely with increasing running time. The summary motion signals during walking were similar to those observed during squatting and jumping. Notably, for the same exercise mode, it can be observed that with the increase of exercise duration, the output voltage presents an amplitude trend, which is ascribed to the change of sweat-induced ionic conductivity because of the increase of sweat ions such as hydronium ions, Na^+, K^+, Ca^{2+}, *etc.*[59] These interesting electrochemical signalling behaviours were also recently reported for the development of triboelectric sweat sensor use in real-time human sweat monitoring.[60,61] The pAd-TENG-based e-skin exhibited features that are promising for the further development of wearable and comfortable self-powered devices capable of reading and displaying the electrical physiological signals of the human body during prolonged daily activities.

Conclusions

Sweating, which occurs inevitably in daily life, greatly reduces interfacial adhesion between a hydrogel electrode and skin, which can lead to the malfunctioning of a healthcare device. To overcome this problem, we exploited the disruptive effect of decreasing sweat pH on the inherent H-bonded network (which promotes protonated states and generates more active groups) to enhance interfacial coupling between a hydrogel electrode and skin. The interfacial toughness, shear strength, and tensile strength of the hydrogel on sweaty skin were observed to increase by factors of 9.7 (453.47 *vs.* 46.74 J m^{-2}), 8.6 (600.14 *vs.* 69.71 MPa), and 10.4 (556.44 *vs.* 53.67 MPa), respectively, with decreasing sweat pH (from 7.5 to 4.5). As a proof-of-concept, stable and reliable electrophysiological signals were recorded from a sweating volunteer when exercising during long-term monitoring using a self-powered e-skin assembled with the CNF/PAA hydrogel electrode. The strategy developed in this study facilitates the design of high-performance adhesive hydrogels for use in self-powered e-skins as intelligent human–machine interfaces.

Experimental section

The detailed experimental section can be found in the ESI.† Informed consent was obtained for publishing the images and data for experiments performed with the assistance of a volunteer.

Author contributions

H. L., D. W. and X. X. conceived the concept, processing, structure details and supervised the work. L. Z. carried out most experiments and wrote the manuscript. H. L., D. W., X. X., and L. Z. revised the manuscript. S. H. W. and Z. M. W. assisted in completing the photographs of samples in the manuscript. Z. H., P. H. S. and F. H. D. contributed to the sample preparation and manuscript editing. All authors commented on the submitted version of the manuscript.

Conflicts of interest

The authors declare no conflict of interest.

Acknowledgements

Notes and references

1 A. Chortos, J. Liu and Z. Bao, *Nat. Mater.*, 2016, **15**, 937.
2 Y. Liu, C. Wang, J. Xue, G. Huang, S. Zheng, K. Zhao, J. Huang, Y. Wang, Y. Zhang, T. Yin and Z. Li, *Adv. Healthcare Mater.*, 2022, **11**, e2200653.
3 C. Wang, X. Qu, Q. Zheng, Y. Liu, P. Tan, B. Shi, H. Ouyang, S. Chao, Y. Zou, C. Zhao, Z. Liu, Y. Li and Z. Li, *ACS Nano*, 2021, **15**, 10130–10140.
4 J. C. Yang, J. Mun, S. Y. Kwon, S. Park, Z. Bao and S. Park, *Adv. Mater.*, 2019, **31**, e1904765.
5 J. Kim, A. S. Campbell, B. E. de Avila and J. Wang, *Nat. Biotechnol.*, 2019, **37**, 389.
6 H. Yuk, J. Wu and X. Zhao, *Nat. Rev. Mater.*, 2022, **7**, 35.
7 Z. Zhang, C. Qin, H. Feng, Y. Xiang, B. Yu, X. Pei, Y. Ma and F. Zhou, *Nat. Commun.*, 2022, **13**, 6964.
8 W. Zhang, B. Wu, S. Sun and P. Wu, *Nat. Commun.*, 2021, **12**, 4082.
9 B. Xue, J. Gu, L. Li, W. Yu, S. Yin, M. Qin, Q. Jiang, W. Wang and Y. Cao, *Nat. Commun.*, 2021, **12**, 7156.
10 C. Wang, Y. Liu, X. Qu, B. Shi, Q. Zheng, X. Lin, S. Chao, C. Wang, J. Zhou, Y. Sun, G. Mao and Z. Li, *Adv. Mater.*, 2022, **34**, e2105416.
11 C. Wang, K. Hu, C. Zhao, Y. Zou, Y. Liu, X. Qu, D. Jiang, Z. Li, M. R. Zhang and Z. Li, *Small*, 2020, **16**, e1904758.
12 S. Nakata, T. Arie, S. Akita and K. Takei, *ACS Sens.*, 2017, **2**, 443.
13 Y. Peng, J. Zhou, Y. Yang, J. C. Lai, Y. Ye and Y. Cui, *Adv. Mater.*, 2022, **34**, e2204168.
14 H. Shen, H. Lei, M. Gu, S. Miao, Z. Gao, X. Sun, L. Sun, G. Chen, H. Huang, L. Chen and Z. Wen, *Adv. Funct. Mater.*, 2022, **32**, 2204525.
15 Q. Zhang, K. Ji, T. Huo, M. N. Khan, Z. Hu, C. Yuan, J. Zhao, J. Chen, Z. Wang and Z. Dai, *ACS Appl. Mater. Interfaces*, 2022, **14**, 48438.
16 H. Zhang, L. Xiang, Y. Yang, M. Xiao, J. Han, L. Ding, Z. Zhang, Y. Hu and L. M. Peng, *ACS Nano*, 2018, **12**, 2773.
17 M. Kaltenbrunner, T. Sekitani, J. Reeder, T. Yokota, K. Kuribara, T. Tokuhara, M. Drack, R. Schwodiauer,

I. Graz, S. Bauer-Gogonea, S. Bauer and T. Someya, *Nature*, 2013, **499**, 458.

18 Y. Yang, Y. Song, X. Bo, J. Min, O. S. Pak, L. Zhu, M. Wang, J. Tu, A. Kogan, H. Zhang, T. K. Hsiai, Z. Li and W. Gao, *Nat. Biotechnol.*, 2020, **38**, 217.

19 J. Cao, X. Yang, J. Rao, A. Mitriashkin, X. Fan, R. Chen, H. Cheng, X. Wang, J. Goh, H. L. Leo and J. Ouyang, *ACS Appl. Mater. Interfaces*, 2022, **14**, 39159.

20 E. P. Chan, E. J. Smith, R. C. Hayward and A. J. Crosby, *Adv. Mater.*, 2008, **20**, 711.

21 J. Yang, R. Bai, B. Chen and Z. Suo, *Adv. Funct. Mater.*, 2019, **30**, 1901693.

22 M. Lin, H. Hu, S. Zhou and S. Xu, *Nat. Rev. Mater.*, 2022, **7**, 850.

23 M. J. Webber and M. W. Tibbitt, *Nat. Rev. Mater.*, 2022, **7**, 541.

24 M. Mesko, L. Xiang, S. Bohle, D. S. Hwang, H. Zeng and M. J. Harrington, *Chem. Mater.*, 2021, **33**, 6530.

25 M. Parrilla, J. Ferré, T. Guinovart and F. J. Andrade, *Electroanalysis*, 2016, **28**, 1267.

26 K. K. Yeung, J. Li, T. Huang, I. I. Hosseini, R. A. Mahdi, M. M. Alam, H. Sun, S. Mahshid, J. Yang, T. T. Ye and Z. Gao, *Nano Lett.*, 2022, **22**, 6647.

27 A. Wiorek, M. Parrilla, M. Cuartero and G. A. Crespo, *Anal. Chem.*, 2020, **92**, 10153–10161.

28 L. Chen, F. Chen, G. Liu, H. Lin, Y. Bao, D. Han, W. Wang, Y. Ma, B. Zhang and L. Niu, *Anal. Chem.*, 2022, **94**, 7319–7328.

29 H. Shen, H. Lei, M. Gu, S. Miao, Z. Gao, X. Sun, L. Sun, G. Chen, H. Huang, L. Chen and Z. Wen, *Adv. Funct. Mater.*, 2022, **32**, 2204525.

30 V. F. Curto, C. Fay, S. Coyle, R. Byrne, C. O'Toole, C. Barry, S. Hughes, N. Moyna, D. Diamond and F. Benito-Lopez, *Sens. Actuators, B*, 2012, **171–172**, 1327–1334.

31 S. Wang, L. Yu, S. Wang, L. Zhang, L. Chen, X. Xu, Z. Song, H. Liu and C. Chen, *Nat. Commun.*, 2022, **13**, 3408.

32 D. Zhao, Y. Zhu, W. Cheng, G. Xu, Q. Wang, S. Liu, J. Li, C. Chen, H. Yu and L. Hu, *Matter*, 2020, **2**, 390.

33 K. Gong, L. Hou and P. Wu, *Adv. Mater.*, 2022, **34**, 2201065.

34 D. Zhao, B. Pang, Y. Zhu, W. Cheng, K. Cao, D. Ye, C. Si, G. Xu, C. Chen and H. Yu, *Adv. Mater.*, 2022, **34**, e2107857.

35 J. Wang, B. Wu, P. Wei, S. Sun and P. Wu, *Nat. Commun.*, 2022, **13**, 4411.

36 X. Q. Wang, K. H. Chan, W. Lu, T. Ding, S. W. L. Ng, Y. Cheng, T. Li, M. Hong, B. C. K. Tee and G. W. Ho, *Nat. Commun.*, 2022, **13**, 3369.

37 P. A. Benitez-Duif, M. Breisch, D. Kurka, K. Edel, S. Gökcay, D. Stangier, W. Tillmann, M. Hijazi and J. C. Tiller, *Adv. Funct. Mater.*, 2022, **32**, 2204837.

38 M. Milovanovic, N. Isselbaecher, V. Brandt and J. C. Tiller, *Chem. Mater.*, 2021, **33**, 8312–8322.

39 Z. Yang, R. Huang, B. Zheng, W. Guo, C. Li, W. He, Y. Wei, Y. Du, H. Wang, D. Wu and H. Wang, *Adv. Sci.*, 2021, **8**, 2003627.

40 Z. Jia, Y. Zeng, P. Tang, D. Gan, W. Xing, Y. Hou, K. Wang, C. Xie and X. Lu, *Chem. Mater.*, 2019, **31**, 5625.

41 Q. Wang, X. Pan, C. Lin, D. Lin, Y. Ni, L. Chen, L. Huang, S. Cao and X. Ma, *Chem. Eng. J.*, 2019, **370**, 1039.

42 Q. Wang, X. Pan, C. Lin, X. Ma, S. Cao and Y. Ni, *Chem. Eng. J.*, 2020, **396**, 125341.

43 Q. Wang, J. Lan, Z. Hua, X. Ma, L. Chen, X. Pan, Y. Li, S. Cao and Y. Ni, *Int. J. Biol. Macromol.*, 2021, **184**, 282.

44 D. Sun, N. Li, J. Rao, S. Jia, Z. Su, X. Hao and F. Peng, *J. Mater. Chem. A*, 2021, **9**, 14381.

45 D. Gan, W. Xing, L. Jiang, J. Fang, C. Zhao, F. Ren, L. Fang, K. Wang and X. Lu, *Nat. Commun.*, 2019, **10**, 1487.

46 Y. Jiao, Y. Lu, K. Lu, Y. Yue, X. Xu, H. Xiao, J. Li and J. Han, *J. Colloid Interface Sci.*, 2021, **597**, 171.

47 D. Gan, Z. Huang, X. Wang, L. Jiang, C. Wang, M. Zhu, F. Ren, L. Fang, K. Wang, C. Xie and X. Lu, *Adv. Funct. Mater.*, 2019, **30**, 1907678.

48 X. Liu, Q. Zhang, L. Duan and G. Gao, *Adv. Funct. Mater.*, 2019, **29**, 1900450.

49 Y. Zhang, W. Zhao, S. Ma, H. Liu, X. Wang, X. Zhao, B. Yu, M. Cai and F. Zhou, *Nat. Commun.*, 2022, **13**, 377.

50 Y. Miao, M. Xu and L. Zhang, *Adv. Mater.*, 2021, **33**, e2102308.

51 Y. Wei, L. Xiang, H. Ou, F. Li, Y. Zhang, Y. Qian, L. Hao, J. Diao, M. Zhang, P. Zhu, Y. Liu, Y. Kuang and G. Chen, *Adv. Funct. Mater.*, 2020, **30**, 2005135.

52 P. Tan, H. Wang, F. Xiao, X. Lu, W. Shang, X. Deng, H. Song, Z. Xu, J. Cao, T. Gan, B. Wang and X. Zhou, *Nat. Commun.*, 2022, **13**, 358.

53 L. Bai, Y. Jin, X. Shang, H. Jin, L. Shi, Y. Li and Y. Zhou, *Nano Energy*, 2022, **104**, 2005135.

54 M. Gao, H. Wu, R. Plamthottam, Z. Xie, Y. Liu, J. Hu, S. Wu, L. Wu, X. He and Q. Pei, *Matter*, 2021, **4**, 1962.

55 H. Jung, M. K. Kim, J. Y. Lee, S. W. Choi and J. Kim, *Adv. Funct. Mater.*, 2020, **30**, 2004407.

56 G. Li, Z. Deng, M. Cai, K. Huang, M. Guo, P. Zhang, X. Hou, Y. Zhang, Y. Wang, Y. Wang, X. Wu and C. F. Guo, *npj Flexible Electron.*, 2021, **5**, 1.

57 Y. Jiang, X. Zhang, W. Zhang, M. Wang, L. Yan, K. Wang, L. Han and X. Lu, *ACS Nano*, 2022, **16**, 8662.

58 X. Chen, H. Yuk, J. Wu, C. S. Nabzdyk and X. Zhao, *Proc. Natl. Acad. Sci. U. S. A.*, 2020, **11**, 15497.

59 M. Bariya, H. Y. Y. Nyein and A. Javey, *Nat. Electron.*, 2018, **1**, 160–171.

60 Y. Qin, J. Mo, Y. Liu, S. Zhang, J. Wang, Q. Fu, S. Wang and S. Nie, *Adv. Funct. Mater.*, 2022, **32**, 2201846.

61 W. Li, L. Lu, A. G. P. Kottapalli and Y. Pei, *Nano Energy*, 2022, **95**, 107018.